Communication

Porcine Skin–Derived Reconstituted Lipid Nanoparticles Intrinsically Boost Fibroblast Proliferation and Migration

Xiangyan Liao and Cheng Wang *

Posted Date: 26 February 2026

doi: 10.20944/preprints202602.1644.v1

Keywords: reconstituted lipid nanoparticles; natural lipids; wound healing

 doi:10.20944/preprints202602.1644.v1

Communication

Porcine Skin–Derived Reconstituted Lipid Nanoparticles Intrinsically Boost Fibroblast Proliferation and Migration

Xiangyan Liao and Cheng Wang *

School of Pharmacy, Changzhou University, Changzhou, Jiangsu 213164, China

* Correspondence: wangc90@cczu.edu.cn

Abstract

Chronic and hard-to-heal wounds remain a major clinical burden, yet many synthetic nanocarriers used in advanced dressings are constrained by limited biomimicry and concerns over inflammatory risk and off-target toxicity. Here we report porcine skin–derived reconstituted lipid nanoparticles (PS-rLNPs) as a tissue-origin, composition-preserving nanoplatform for wound repair. Total lipids extracted from fresh porcine skin were assembled into nanoparticles via a facile solvent-injection process. Lipidomics revealed a triglyceride- and phosphatidylcholine-dominant composition accompanied by minor membrane-relevant lipid species, suggesting a biocompatible, multi-lipid milieu. PS-rLNPs formed a stable nanoscale dispersion and maintained colloidal stability in physiologically relevant and serum-containing media. In vitro, PS-rLNPs showed no cytotoxicity across the tested dose range and exhibited pronounced intrinsic pro-healing bioactivity, significantly enhancing fibroblast viability and accelerating cell motility in both scratch-closure and Transwell migration assays. Collectively, these results establish PS-rLNPs as a biocompatible, serum-stable, and intrinsically pro-regenerative lipid nanoparticle system, providing a scalable route to tissue-derived nanomedicines that may complement next-generation wound-care strategies.

Keywords: reconstituted lipid nanoparticles; natural lipids; wound healing

1. Introduction

Wound healing is a critical physiological process essential for maintaining skin integrity and preventing life-threatening complications, yet it remains a global clinical challenge [1–3]. It was reported that chronic non-healing wounds affect 10.5 million U.S. Medicare beneficiaries (up 2.3 million from 2014) and nearly 2.5% of the total U.S. population, causing high morbidity and mortality [4], imposing a substantial burden on patients and healthcare systems [5,6]. Acute wounds typically follow a well-orchestrated cascade (hemostasis, inflammation, proliferation, remodeling), but disruptions—due to aging, diabetes, or immunosuppression—often lead to chronicity [7,8]. These non-healing wounds exhibit prolonged inflammation, impaired angiogenesis, and bacterial infection, significantly increasing morbidity (e.g., amputations) and mortality risks [9,10]. Conventional dressings (e.g., gauze) merely provide basic coverage, failing to modulate the healing microenvironment or accelerate tissue regeneration [11,12]. Thus, developing advanced wound dressings that address these unmet needs is imperative to improve patient quality of life, reduce healthcare expenditures, and mitigate the clinical burden of impaired wound repair [13,14].

In recent years, research efforts have centered on integrating nanocarriers as core delivery platforms in wound dressings to accelerate wound healing, with polymer-based nanoparticles [15,16], liposomes [17,18], and metal organic frameworks [19,20] being extensively investigated. These systems are favored for their cost-effectiveness and facile surface modification, which enable tailored loading of bioactive molecules for wound-relevant functions (e.g., anti-inflammation, tissue regeneration). Yet they suffer from inherent limitations that hinder clinical translation: they often

 doi:10.20944/preprints202602.1644.v1

induce considerable hepatorenal toxicity, trigger off-target inflammatory responses, and exhibit non-negligible immunogenicity, particularly upon long-term or high-dose application. Over the same period, biomimetic natural nanocarriers—most notably mammalian cell-derived exosome—have garnered significant attention for treating diverse diseases, owing to their inherent tissue-homing capability, excellent biocompatibility, and minimal cytotoxicity [21,22]. Previous reports have shown that the use of mesenchymal stem cell exosomes in the immunomodulatory treatment of skin regeneration yielded satisfactory results [23], while adipose-derived stem cell exosomes can significantly accelerate wound repair [24]. Despite these advantages, exosomes face formidable translational barriers that limit their widespread use: (i) extremely low production yields, which restrict scalable manufacturing [25]; (ii) labor-intensive and time-consuming isolation/purification processes that increase production costs [26]; (iii) poor batch-to-batch homogeneity, leading to inconsistent therapeutic efficacy [27]; and (iv) residual extraneous proteins and nucleic acids from parent cells, which pose risks of unintended immunogenicity or toxicity [28].

To address these challenges, in previous studies, we proposed the concept and preparation of reconstituted lipid nanoparticles (rLNPs)—a unified platform defined by a core design paradigm: extracting lipids from natural sources (food matrices, plant tissues, mammalian cells/tissues) and fabricating nanoparticles via a facile, reproducible solvent-diffusion method [29–31]. This design preserves the source-specific lipid compositions that endow rLNPs with inherent functional advantages, while ensuring high biocompatibility (negligible hemolysis, low cytotoxicity) and adaptive functionality across various applications. For example, brain-derived rLNPs exhibited selective homing to ischemic tissue and anti-inflammatory/anti-apoptotic effects, underscoring rLNPs' potential to target wound-damaged regions and mitigate pathological inflammation that impairs healing [14]. Additionally, celery seed-derived rLNPs inherently targeted neurons and exerted neuroprotective effects via anti-inflammatory pathways, leveraging natural lipid components to modulate tissue repair microenvironments—an attribute transferable to regulating wound inflammatory cascades [32]. Moreover, cell/tissue-derived rLNPs efficiently loaded hydrophilic/hydrophobic drugs and showed high biocompatibility, proving the platform's capacity to deliver diverse active molecules without cytotoxicity [31]. Collectively, these studies establish rLNPs as a versatile platform: their lipid-source-driven bioactivity (anti-inflammation, bioactive protection), tissue-targeting potential, and broad payload adaptability directly address key wound repair challenges, making them a compelling candidate for wound repair.

Against this background, we hypothesized that skin-tissue–derived lipid compositions could be leveraged to create an intrinsically bioactive, biomimetic nanoplatform for wound repair while avoiding key limitations of vesicle-based therapies, including production complexity and batch heterogeneity. To test this hypothesis, we extracted total lipids from fresh porcine skin and fabricated PS-rLNPs via a simple solvent-injection strategy, followed by comprehensive physicochemical characterization spanning composition, morphology, size distribution, and stability in protein-rich environments relevant to wound exudates. We then evaluated biosafety and intrinsic pro-healing potential using fibroblasts as key effector cells in wound closure, quantitatively assessing proliferation and motility using viability assays, live/dead imaging, scratch healing, and Transwell migration. This work therefore proposes a tissue-origin rLNP paradigm for wound care, in which composition-informed design and colloidal robustness jointly enable an inherently bioactive lipid nanoplatform.

2. Materials and Methods

2.1. Materials and Chemical Reagents

Fresh pig skin was purchased from a local market. Methyl tert-butyl ether (MTBE) and methanol (MeOH) were obtained from Shanghai Titan Technology Co., Ltd. (Shanghai, China). Anhydrous ethanol, dichloromethane (DCM), and paraformaldehyde were purchased from Sinopharm Chemical Reagent Co., Ltd. (Shanghai, China). Dulbecco's Modified Eagle Medium (DMEM), fetal bovine

 doi:10.20944/preprints202602.1644.v1

serum (FBS), and phosphate-buffered saline (PBS) were from Servicebio Biotechnology Co., Ltd. (Guangzhou, China). Penicillin-Streptomycin (Pen-Strep) and 0.25% trypsin were from Beyotime Biotechnology Co., Ltd. (Shanghai, China). All other reagents used were of analytical grade or higher.

2.2. Preparation and Characterization of PS-rLNPs

2.2.1. Extraction and Component Analysis of Pig Skin Lipids

To ensure the batch-to-batch stability and consistency of porcine skin-derived lipids and subsequent lipid nanoparticles (LNPs), a systematic control strategy was implemented throughout the extraction process. All fresh pig skin was sourced from a single fixed supplier, selecting skin from healthy pigs of the same breed and growth cycle (6–8 months); within one hour of acquisition, impurities such as fascia, hair, and subcutaneous fat were removed, followed by three rapid rinses with sterile normal saline to ensure uniform initial lipid composition across batches. The treated pig skin was cut into small pieces, mixed with MTBE:MeOH (3:1, v/v) at a fixed ratio, and subjected to magnetic stirring in a 4 ℃ water bath for 2 h. Subsequently, H_2O:MeOH (3:1, v/v) was added, and the mixture was allowed to stand for phase separation. The upper organic phase was collected and subjected to rotary evaporation to remove solvents; the residue was resuspended in dichloromethane (DCM), followed by centrifugation at 12,000 rpm (4 °C) for 10 min. The supernatant was discarded, and the precipitated lipid fraction was nitrogen-dried, then further vacuum-dried to obtain lipid products.

2.2.2. Preparation of PS-rLNPs

PS-rLNPs were prepared via the solvent injection method. Briefly, total lipids extracted from pig skin were dissolved in anhydrous ethanol (15 mg/mL), sonicated (300 W, 5 min), and filtered through a 0.22 μm membrane. This ethanolic solution was then rapidly injected into pure water under vigorous stirring (1500 rpm) to form the nanoparticles.

2.2.3. Characterization of Nanoparticles

The particle size distribution (Z-Average, Number Size) and polydispersity index (PDI) of PS-rLNPs were determined using a Malvern Zetasizer Nano (Malvern, UK). For morphological observation, samples were diluted with ultrapure water to 1 mg/mL, negatively stained with phosphotungstic acid, deposited on a carbon-coated copper grid, and dried for morphological observation using a transmission electron microscope (TEM Tecnai G20, FEI, USA). To evaluate the stability of PS-rLNPs in a physiological environment, the nanoparticles were mixed with ultrapure water or complete cell culture medium at a volume ratio of 1:2 (final concentration: 200 μg/mL) and placed at room temperature. The Number Size and PDI were monitored over 7 consecutive days using a Malvern Zetasizer.

2.3. In Vitro Experiments

2.3.1. Cell Culture

Murine fibroblast cell lines 3T3 and L929 were used in the experiment. Cells were cultured in DMEM supplemented with 10% fetal bovine serum (FBS) and 1% Pen-Strep, in a 37 ℃, 5% CO_2 incubator. Cells in the logarithmic growth phase were employed for all subsequent experiments.

2.3.2. Cell Proliferation

The MTT assay was employed to evaluate the effect of PS-rLNPs on cell proliferation. Cells were seeded into 96-well plates at a density of 2×10^3 cells/well and cultured for 24 h to allow adherence. The medium was then replaced with fresh medium containing PS-rLNPs at concentrations of 100, 200, 300, 400, and 500 μg/mL (200 μL/well). Each concentration was set in 5 replicate wells. After 24

 doi:10.20944/preprints202602.1644.v1

h of treatment, 20 μL of 5 mg/mL MTT solution was added, and the plates were incubated at 37 ℃ with 5% CO_2 for 4 h. Afterward, the medium was aspirated, and DMSO was added to dissolve formazan crystals. The absorbance was measured at 570 nm using a microplate reader (Synergy NEO, BioTek, USA). Blank wells (medium only) and negative control wells (cells + medium without PS-rLNPs) were set up. Cell viability was calculated using the following formula:

$$Cell\ viability\ (\%) = \frac{A_{sample} - A_{blank}}{A_{control} - A_{blank}} \times 100\%$$

Where A_{sample}, $A_{control}$, and A_{blank} are the absorbance values of the PS-rLNPs-treated group, control group, and blank group, respectively.

The effect of PS-rLNPs on cell viability was evaluated using a Calcein-AM staining kit (KeyGen BioTECH, Nanjing, China). Cells were seeded into 6-well plates at a density of 5×10^4 cells/well and allowed to adhere. The medium was replaced with cell culture medium containing 300 μg/mL PS-rLNPs, and the cells were treated for 24 h. Staining was performed according to the manufacturer's instructions. Observations and imaging were conducted using a laser confocal microscope (Nikon Eclipse Ti2, Nikon Corporation, Japan).

2.3.3. Cell Migration (Scratch & Transwell Assays)

Cell scratch assay and Transwell migration assay were used to evaluate the effect of PS-rLNPs on the migratory capacity of fibroblasts (3T3/L929).

3T3/L929 cells were seeded into 6-well plates and cultured until confluent. Scratches were created using a sterile pipette tip, and after washing with PBS, the experimental group was supplemented with low-serum medium (2% FBS) containing 300 μg/mL PS-rLNPs, while the control group received an equal volume of blank low-serum medium (2% FBS). Images of the scratch areas were captured at 0 h and 24 h using an inverted fluorescence microscope (Eclipse Ti-S, Nikon Corporation, Japan). The scratch width was measured via ImageJ software, and the migration rate was calculated using the following formula:

$$Migration\ rate\ (\%) = \frac{W_0 - W_{24}}{W_0} \times 100\%$$

Where W_0 and W_{24} are the scratch widths at 0 h and 24 h, respectively.

For the Transwell assay, the lower chamber was loaded with complete medium containing 10% FBS as a chemoattractant. The upper chamber was filled with serum-free cell suspension (5×10^5 cells/mL) with 300 μg/mL PS-rLNPs (experimental group) or without PS-rLNPs (control group). After 24 h of culture, cells were fixed with 4% paraformaldehyde, stained with 0.1% crystal violet, and non-migrated cells in the upper chamber were gently removed. The number of migrated cells was counted by randomly selecting five fields of view per membrane under an inverted fluorescence microscope (Eclipse Ti-S, Nikon Corporation, Japan) [33].

3. Results and Discussion

3.1. Preparation and Physical Characterization of PS-rLNPs

The physicochemical properties of PS-rLNPs were first investigated, which is the basis for verifying whether they can be used for wound healing applications. In this study, fresh pig skin was used for the raw material, and a modified MTBE/MeOH system was adopted to extract total lipids. By optimizing the solvent ratio and extraction temperature, this extraction system enhanced the lipid dissolution efficiency, laying the foundation for the subsequent preparation of nanoparticles. PS-rLNPs were prepared by the ethanol injection method, with the preparation process and product morphological characteristics illustrated in Figure 1A.

LC-MS lipidomic analysis showed that PS-rLNPs are mainly composed of triglycerides (TG, 77.9%) and phosphatidylcholine (PC, 11.6%) (Figure 1B). The remaining lipid components are sphingomyelin (SM, 3.2%), phosphatidylethanolamine (PE, 2%), diglycerides (DG, 1.2%), cholesterol

 doi:10.20944/preprints202602.1644.v1

esters (ZyE, 0.8%), sphingosine (So, 0.7%), lysophosphatidylcholine (LPC, 0.5%), and monoglycerides (MG, 0.4%). This composition has important dual biological significance. On the one hand, as a key structural lipid of biological cell membranes, PC has a hydrophilic head and hydrophobic tail, which can enhance the compatibility of nanoparticles with biological membranes, facilitate nanoparticles to cross biological membrane barriers, and improve delivery efficiency [34]. On the other hand, as an energy storage substance, TG can provide energy for cell metabolism during wound healing and coordinately regulate signaling pathways related to cell proliferation and differentiation [35]. In addition, other components in PS-rLNPs also play important roles: SM and So can form "lipid rafts" to enhance membrane stability and signal transduction [36,37]; PE can promote membrane fusion and autophagy; MG can act as second messengers to activate related signaling pathways [38]; LPC can recruit immune cells in the early stage of inflammation [39]; ZyE can exert anti-inflammatory effects and regulate the repair process [40]. These components work synergistically with PC and TG, making PS-rLNPs an "intelligent" therapeutic system with active repair functions, providing a theoretical basis for its application in the field of wound repair. The detailed roles of these lipids in the functionality of PS-rLNPs remain to be investigated in our future works.

PS-rLNPs were fabricated by the ethanol injection method. The PS-rLNPs aqueous solution appeared as uniform"translucent milky white colloid", and the Tyndall effect was observed under laser irradiation, confirming that the nanoscale particles were stably dispersed without obvious agglomeration (Figure 1C). Dynamic light scattering (DLS) characterization showed (Figure 1D) that the hydrated particle size of PS-rLNPs was 91.3 nm (PDI = 0.225), which falls within the optimal size range (< 200 nm) as efficient delivery systems. Transmission electron microscopy (TEM) further demonstrated a monodisperse spherical dehydrated morphology (Figure 1E), with regular particle morphology and no interparticle adhesion, and an average diameter of approximately 40 nm. It should be noted that this size is smaller than the hydrated particle size measured by DLS [41]. This discrepancy is likely attributed to DLS measuring the size of the hydrated shell of nanoparticles in aqueous solution, while TEM measures the size of the dehydrated particle core. Dehydration shrinkage leads to differences between the two, which is consistent with the general principles of nanoparticle characterization.

Considering the clinical application potential of PS-rLNPs, evaluating their stability in simulated physiological environments is essential. In the experiment, aqueous medium with pH 7.4 (simulating the pH environment of body fluids) and cell culture medium containing 10% fetal bovine serum (FBS, simulating the *in vivo* protein environment) were selected as the test systems, and the particle size changes of PS-rLNPs at different time points were monitored by DLS (Figure 1F). In pH 7.4 ultrapure water, the particle size of PS-rLNPs remained in the range of 75–102 nm within 7 days, and the PDI value was less than 0.25; in the cell culture medium containing 10% FBS, the particle size fluctuation range was 91–103 nm, and the PDI value was less than 0.30. The above results indicate that PS-rLNPs have excellent stability in the simulated physiological environment and can still maintain a stable particle size and low PDI in serum-containing medium, indicating favorable colloidal stability for *in vivo* applications.

 doi:10.20944/preprints202602.1644.v1

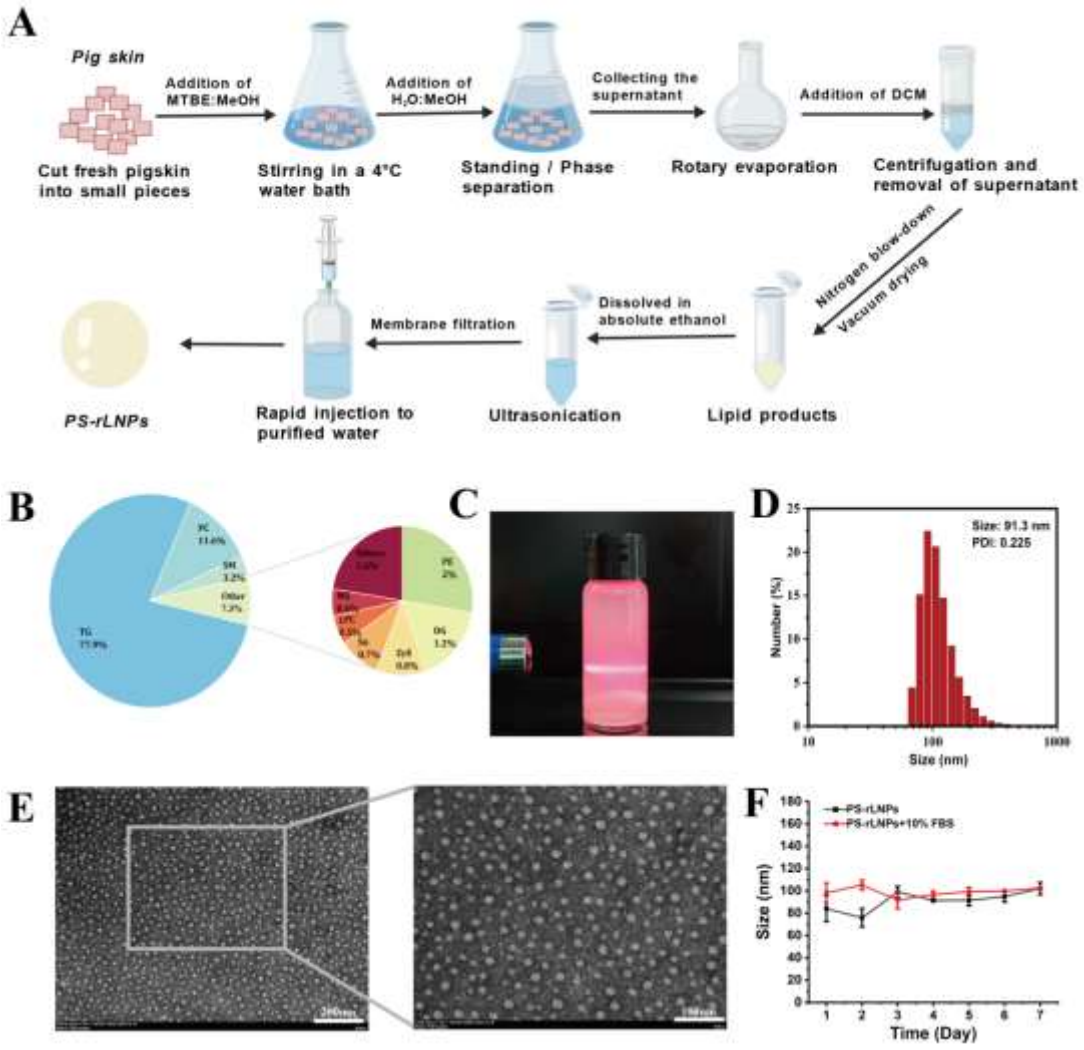

Figure 1. Preparation and characterization of PS-rLNPs. (A) Schematic diagram of the process for extracting lipids from pig skin and preparing PS-rLNPs. (B) Pie chart showing the relative content of main lipid components in PS-rLNPs. (C) Photograph of the prepared PS-rLNPs aqueous dispersion. (D) Hydrodynamic particle size distribution diagram of PS-rLNPs. (E) TEM image of PS-rLNPs; the inset shows the high-resolution morphology of a single nanoparticle. Scale bar: 200 nm, 100 nm. (F) Stability evaluation of PS-rLNPs stored in *p*H 7.4 water and cell culture medium containing 10% FBS. Data are expressed as mean ± standard deviation (n = 3).

3.2. In Vitro Biological Effects of PS-rLNPs

Following the physicochemical characterization of PS-rLNPs, further verification of their biological safety and inherent pro-healing activity is essential. This is the key prerequisite for wound treatment: they must be non-toxic and have the ability to promote cell proliferation/migration. In this section, MTT assay, live/dead staining, and scratch assay were used to systematically evaluate the effects of PS-rLNPs on fibroblasts (core cells involved in wound healing), providing *in vitro* evidence for subsequent *in vivo* experiments [42].

To systematically evaluate the biological safety and bioactivity of PS-rLNPs, the MTT assay was first used to detect their effects on the survival and proliferation of 3T3 fibroblasts (Figure 2A). Within the concentration range of 0–500 μg/mL, PS-rLNPs exhibited no cytotoxicity and exhibited concentration-dependent pro-cell proliferation activity: when the concentration increased to 300 μg/mL, the viability of 3T3 cells reached the maximum level of 153.3%, while a further increase to 500 μg/mL resulted in a slight decrease in viability (145.4%). These results indicate that PS-rLNPs are

 doi:10.20944/preprints202602.1644.v1

non-toxic and can actively promote fibroblast proliferation. Considering both bioactivity and practicality, 300 μg/mL was identified as the optimal concentration. Therefore, this concentration was used in subsequent experiments unless otherwise stated.

To verify the cell universality of this effect, the same experiment was conducted on another fibroblast cell line L929. As shown in Figure. S1, the viability of L929 also reached a maximum of 157.5% at a PS-rLNPs concentration of 300 μg/mL. This stands in stark contrast to the cellular inhibitory effects of many traditional synthetic nanomaterials at high concentrations, thereby highlighting the biocompatibility advantage of natural lipid-based components. Many synthetic nanomaterials are prone to cause cellular oxidative stress or membrane damage at high concentrations due to issues such as surface charge and agglomeration, leading to cell inhibition or even death. However, PS-rLNPs, leveraging the inherent biocompatibility of their natural lipid components (e.g., PC and TG), achieve safe pro-proliferative effects at high concentrations, addressing a key safety concern for their clinical translation.

To further corroborate the findings of the MTT assay, a live/dead cell staining experiment was conducted to enable direct visualization of cell viability (Figure 2B, S2). Specifically, the optimal concentration of PS-rLNPs (300 μg/mL) identified in the MTT assay was selected for validation, with no concentration gradient established in this experiment. Under fluorescence microscopy, the PS-rLNPs-treated group (300 μg/mL) displayed dense green fluorescence, which corresponded to viable cells stained with calcein. In contrast, the density of green fluorescent cells in the control group was significantly lower than that in the PS-rLNPs-treated group. This visual evidence is highly consistent with the quantitative data obtained from the MTT assay, further confirming that PS-rLNPs exhibit no cytotoxicity and can effectively promote cell proliferation at a concentration of 300 μg/mL.

Given that the migration ability of fibroblasts, which are responsible for filling wound defects and secreting extracellular matrix, plays important roles in wound healing, the scratch assay was used to evaluate the regulatory effect of 300 μg/mL PS-rLNPs on the migration of 3T3 and L929 cells. In the experiment, a “scratch” of uniform width was created on the cell monolayer, and the healing of the scratch area was monitored at 24 h post treatment. The data showed that after 24 h of culture, the scratch healing rate of 3T3 cells in the PS-rLNPs treatment group reached 43.65%, which was significantly higher than that of the control group (20.75%). The scratch area was rapidly covered by migrated fibroblasts, with distinct cell migration phenotypes (Figure 2C, D). Similarly, the healing rate of L929 cells treated with PS-rLNPs reached 28.19%, which was higher than that of the control group (5.68%) (Figure S3).

To further confirm the cell migratory capacity, the Transwell assay (Boyden chamber method) was employed (Figure 2E, F). In the experiment, PS-rLNPs were added to the Transwell chamber, and after treatment with PS-rLNPs, more 3T3 cells migrated to the lower surface of the Transwell membrane. Quantitative counting revealed that the number of migrated cells in the PS-rLNPs treatment group was 510 cells per field of view, which was significantly higher than that in the control group (350 cells per field of view), with an extremely significant statistical difference ($p < 0.001$) (Figure 2G). Consistent results were obtained when L929 cells were used (Figure S4**).** This result excludes the influence of cell proliferation, directly confirming that PS-rLNPs can significantly enhance the migration ability of fibroblasts, providing key experimental evidence for the subsequent investigation of PS-rLNPs in wound repair.

 doi:10.20944/preprints202602.1644.v1

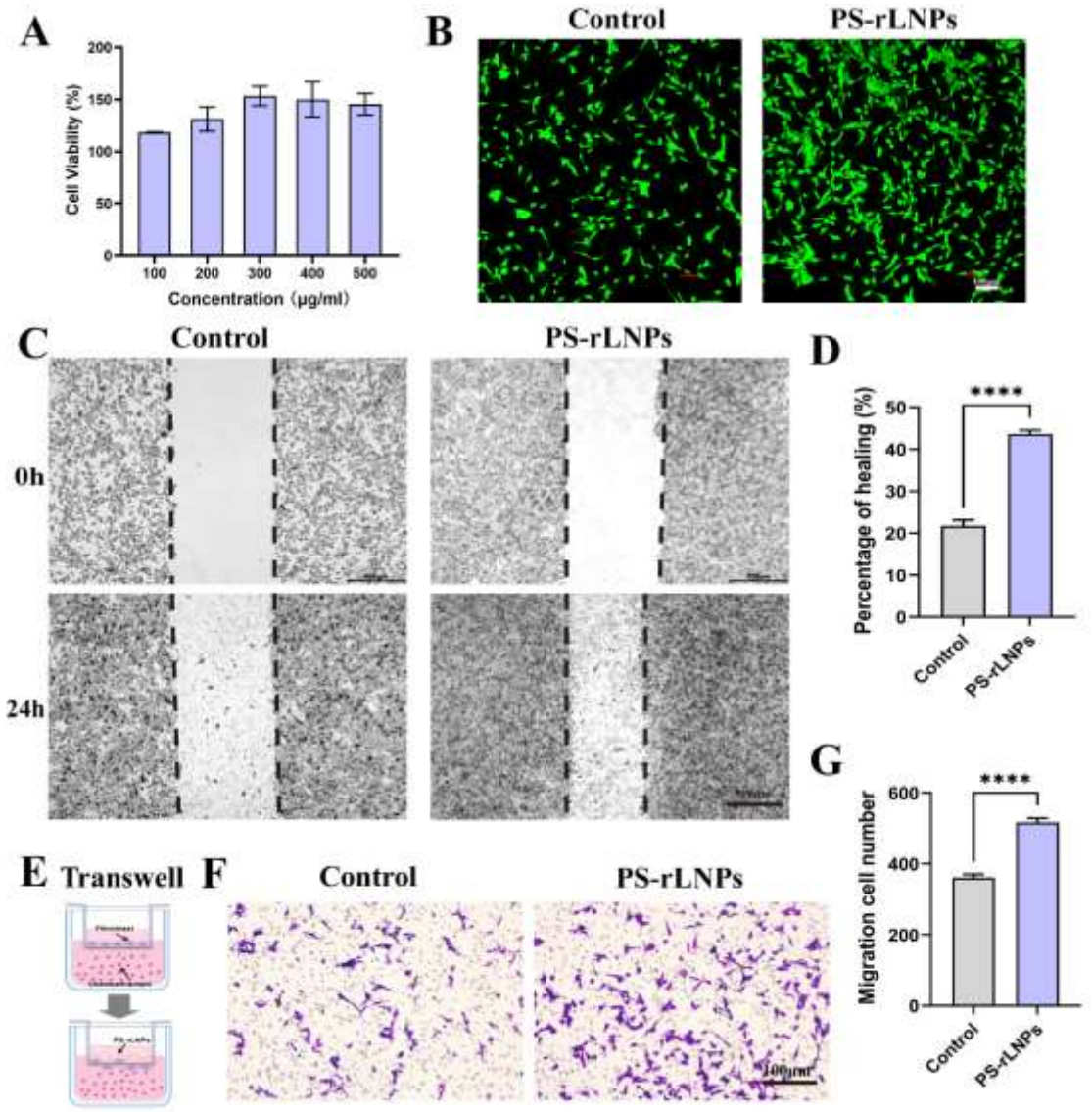

Figure 2. *In vitro* biological effects of PS-rLNPs on 3T3 cells. (A) Cell viability of 3T3 cells treated with different concentrations of PS-rLNPs (determined by MTT assay). (B) Representative images of live cell staining (Calcein-AM, green fluorescence). Scale bar: 100 μm. (C) Representative images of the scratch assay of 3T3 cells at 0 h and 24 h for evaluating cell migration ability. Scale bar: 500 μm. (D) Quantitative statistical analysis of the scratch area healing rate in (C). (E) Schematic diagram of the Transwell assay device. (F) Representative images of crystal violet staining of 3T3 cells that migrated through the polycarbonate membrane in the Transwell chamber migration assay. Scale bar: 100 μm. (G) Quantitative statistical analysis of the number of migrated cells in (F). Data are expressed as mean ± standard deviation (*$p < 0.05$, **$p < 0.01$, ***$p < 0.001$, ****$p < 0.0001$ compared with the Control group, n = 3).

4. Conclusion

This study advances a tissue-origin strategy for wound-healing nanomedicine by demonstrating that reconstituted nanoparticles assembled from porcine skin lipids can function as more than passive carriers. Instead, PS-rLNPs behave as an intrinsically bioactive lipid ensemble that amplifies two cellular programs central to repair—fibroblast expansion and directed motility—under conditions compatible with protein-rich biological media. These findings suggest that the regenerative activity of lipid nanoparticles can be "encoded" at the level of native lipid composition, offering a complementary design axis to conventional approaches that rely primarily on loaded drugs, synthetic polymers, or single-component liposomes.

 doi:10.20944/preprints202602.1644.v1

Beyond the immediate wound-care context, the PS-rLNP framework highlights a generalizable principle: tissue-derived lipidomes can be reconstructed into stable nanoscale materials that retain functional cues relevant to the tissue of origin, potentially enabling a new class of biomimetic, scalable nanoplatforms. At the same time, several questions emerge that will define the translational path forward, including identifying the lipid species and downstream signaling networks most responsible for the observed pro-migratory phenotype, clarifying how the wound microenvironment modulates nanoparticle–protein coronas and cellular uptake, and establishing efficacy and safety in clinically relevant wound models with standardized dosing and formulation for topical delivery. Taken together, PS-rLNPs provide a practical and conceptually distinct route toward tissue-informed nanotherapeutics, where composition-guided reconstruction and biological robustness converge to support regenerative medicine applications.

Supplementary Materials: The following supporting information can be downloaded at the website of this paper posted on Preprints.org.

Data availability: Data will be made available on request.

Acknowledgments: The authors acknowledge the funding support from Jiangsu Provincial Young Science and Technology Talents Support Project (No. JSTJ-2025-774) and Changzhou Young Scientific and Technological Talent Support Program (No. CZTJ-2025-05). We acknowledge Zhenjiang Zhuan Bo Testing Technology Co., Ltd. for providing the TEM results, OE Biotech (Shanghai, China) for performing the professional lipidomic analysis, and the schematic drawing service provided by Figdraw.

Declaration of competing interest: The authors declare that they have no known competing financial interests or personal relationships that could have appeared to influence the work reported in this paper.

Declaration of AI and AI-assisted technologies in the writing process: During the preparation of this work the authors used [Doubao AI / DeepSeek] in order to enhance the readability of the manuscript, address grammatical issues, and refine the language. After using this tool/service, the authors reviewed and edited the content as needed and take full responsibility for the content of the publication.

Reference

1. G.C. Gurtner, S. Werner, Y. Barrandon, M.T. Longaker, Wound repair and regeneration, Nature 453(7193) (2008) 314-321.
2. C.K. Sen, Human wound and its burden: updated 2020 compendium of estimates, Advances in wound care 10(5) (2021) 281-292.
3. H. Sorg, D.J. Tilkorn, S. Hager, J. Hauser, U. Mirastschijski, Skin wound healing: an update on the current knowledge and concepts, European surgical research 58(1-2) (2017) 81-94.
4. C.K. Sen, Human Wound and Its Burden: Updated 2022 Compendium of Estimates, Advances in Wound Care 12(12) (2023) 657-670.
5. M. Olsson, K. Järbrink, U. Divakar, R. Bajpai, Z. Upton, A. Schmidtchen, J. Car, The humanistic and economic burden of chronic wounds: a systematic review, Wound repair and regeneration 27(1) (2019) 114-125.
6. J.F. Guest, N. Ayoub, T. McIlwraith, I. Uchegbu, A. Gerrish, D. Weidlich, K. Vowden, P. Vowden, Health economic burden that wounds impose on the National Health Service in the UK, BMJ open 5(12) (2015) e009283.
7. G. Han, R. Ceilley, Chronic wound healing: a review of current management and treatments, Advances in therapy 34(3) (2017) 599-610.
8. L. Cañedo-Dorantes, M. Cañedo-Ayala, Skin acute wound healing: a comprehensive review, International journal of inflammation 2019(1) (2019) 3706315.
9. R.G. Frykberg, J. Banks, Challenges in the treatment of chronic wounds, Advances in wound care 4(9) (2015) 560-582.

 doi:10.20944/preprints202602.1644.v1

10. V. Falanga, R.R. Isseroff, A.M. Soulika, M. Romanelli, D. Margolis, S. Kapp, M. Granick, K. Harding, Chronic wounds, Nature Reviews Disease Primers 8(1) (2022) 50.
11. E. Rezvani Ghomi, M. Niazi, S. Ramakrishna, The evolution of wound dressings: From traditional to smart dressings, Polymers for Advanced Technologies 34(2) (2023) 520-530.
12. L. Long, W. Liu, C. Hu, L. Yang, Y. Wang, Construction of multifunctional wound dressings with their application in chronic wound treatment, Biomaterials science 10(15) (2022) 4058-4076.
13. M. Farahani, A. Shafiee, Wound healing: from passive to smart dressings, Advanced Healthcare Materials 10(16) (2021) 2100477.
14. D. Han, M. Wang, N. Dong, J. Zhang, D. Li, X. Ma, Y. Ma, S. Wang, Y. Zhu, C. Wang, Selective homing of brain-derived reconstituted lipid nanoparticles to cerebral ischemic area enables improved ischemic stroke treatment, Journal of Controlled Release 365 (2024) 957-968.
15. X. Fang, Y. Liu, M. Zhang, S. Zhou, P. Cui, H. Hu, P. Jiang, C. Wang, L. Qiu, J. Wang, Glucose oxidase loaded thermosensitive hydrogel as an antibacterial wound dressing, Journal of Drug Delivery Science and Technology 76 (2022) 103791.
16. T.T.P. Ho, H.A. Tran, V.K. Doan, J. Maitz, Z. Li, S.G. Wise, K.S. Lim, J. Rnjak-Kovacina, Natural Polymer-Based Materials for Wound Healing Applications, Advanced NanoBiomed Research 4(5) (2024) 2300131.
17. Q. Ding, C. Ding, X. Liu, Y. Zheng, Y. Zhao, S. Zhang, S. Sun, Z. Peng, W. Liu, Preparation of nanocomposite membranes loaded with taxifolin liposome and its mechanism of wound healing in diabetic mice, International Journal of Biological Macromolecules 241 (2023) 124537.
18. T. Aparecida Nunes Ribeiro, D. Crístian Ferreira Soares, G. Aparecida dos Santos, M.C. Lino de Souza, B. Xavier Gonçalves, P. Fernanda da Silva Valentim, M. Oliveira de Paula, D. Sachs, Liposomes applied in healing bacterially infected wounds: a systematic review, Journal of Liposome Research (2025) 1-17.
19. C. Wang, R. Xiao, Q. Yang, J. Pan, P. Cui, S. Zhou, L. Qiu, Y. Zhang, J. Wang, Green synthesis of epigallocatechin gallate-ferric complex nanoparticles for photothermal enhanced antibacterial and wound healing, Biomedicine & Pharmacotherapy 171 (2024) 116175.
20. A. Bigham, N. Islami, A. Khosravi, A. Zarepour, S. Iravani, A. Zarrabi, MOFs and MOF-based composites as next-generation materials for wound healing and dressings, Small 20(30) (2024) 2311903.
21. Y. An, S. Lin, X. Tan, S. Zhu, F. Nie, Y. Zhen, L. Gu, C. Zhang, B. Wang, W. Wei, Exosomes from adipose-derived stem cells and application to skin wound healing, Cell proliferation 54(3) (2021) e12993.
22. C. Zhou, B. Zhang, Y. Yang, Q. Jiang, T. Li, J. Gong, H. Tang, Q. Zhang, Stem cell-derived exosomes: emerging therapeutic opportunities for wound healing, Stem cell research & therapy 14(1) (2023) 107.
23. N. Su, Y. Hao, F. Wang, W. Hou, H. Chen, Y. Luo, Mesenchymal stromal exosome–functionalized scaffolds induce innate and adaptive immunomodulatory responses toward tissue repair, Science advances 7(20) (2021) eabf7207.
24. Y. Song, Y. You, X. Xu, J. Lu, X. Huang, J. Zhang, L. Zhu, J. Hu, X. Wu, X. Xu, Adipose-derived mesenchymal stem cell-derived exosomes biopotentiated extracellular matrix hydrogels accelerate diabetic wound healing and skin regeneration, Advanced Science 10(30) (2023) 2304023.
25. R. Zhang, T. Bu, R. Cao, Z. Li, C. Wang, B. Huang, M. Wei, L. Yuan, G. Yang, An optimized exosome production strategy for enhanced yield while without sacrificing cargo loading efficiency, Journal of Nanobiotechnology 20(1) (2022) 463.
26. J.J. Lai, Z.L. Chau, S.Y. Chen, J.J. Hill, K.V. Korpany, N.W. Liang, L.H. Lin, Y.H. Lin, J.K. Liu, Y.C. Liu, Exosome processing and characterization approaches for research and technology development, Advanced Science 9(15) (2022) 2103222.
27. C. Paganini, H. Boyce, G. Libort, P. Arosio, High-yield production of extracellular vesicle subpopulations with constant quality using batch-refeed cultures, Advanced Healthcare Materials 12(8) (2023) 2202232.
28. Y. Xia, J. Zhang, G. Liu, J. Wolfram, Immunogenicity of extracellular vesicles, Advanced materials 36(33) (2024) 2403199.
29. Q. Ge, J. Zhang, Y. Wang, J. Liu, H. Hu, W. Wang, C. Wang, Pickering emulsion stabilized by soy lecithin-derived lipid nanoparticles to amplify the antimicrobial and anti-inflammatory functions of rose essential oil, Food Research International (2025) 117081.

 doi:10.20944/preprints202602.1644.v1

30. D. Han, L. Ji, M. Lu, D. Li, X. Sheng, J. Zhang, C. Wang, Pickering emulsion stabilized by egg derived reconstituted lipid nanoparticles for encapsulation and oral delivery of curcumin, Food Chemistry 472 (2025) 142912.
31. C. Wang, Reconstituted lipid nanoparticles from cells/tissues for drug delivery in cancer, Molecular Pharmaceutics 20(6) (2023) 2891-2898.
32. D. Han, J. Zhang, D. Li, C. Wang, Celery seed derived reconstituted lipid nanoparticles as an innate neuron-targeted neuroprotective nanomedicine for ischemic stroke treatment, Journal of Nanobiotechnology 23(1) (2025) 298.
33. J. Che, D. Huang, Y. Wang, G. Gao, Y. Zhao, Natural multi-active nanoparticles integrated biological hydrogel microcarriers for wound healing, Journal of Nanobiotechnology 23(1) (2025) 582.
34. G. Van Meer, D.R. Voelker, G.W. Feigenson, Membrane lipids: where they are and how they behave, Nature reviews Molecular cell biology 9(2) (2008) 112-124.
35. Z. Wang, F. Zhao, C. Xu, Q. Zhang, H. Ren, X. Huang, C. He, J. Ma, Z. Wang, Metabolic reprogramming in skin wound healing, Burns & Trauma 12 (2024) tkad047.
36. J.A. Hengst, J.M. Guilford, T.E. Fox, X. Wang, E.J. Conroy, J.K. Yun, Sphingosine kinase 1 localized to the plasma membrane lipid raft microdomain overcomes serum deprivation induced growth inhibition, Archives of biochemistry and biophysics 492(1-2) (2009) 62-73.
37. S. Asano, K. Kitatani, M. Taniguchi, M. Hashimoto, K. Zama, S. Mitsutake, Y. Igarashi, H. Takeya, J. Kigawa, A. Hayashi, Regulation of cell migration by sphingomyelin synthases: sphingomyelin in lipid rafts decreases responsiveness to signaling by the CXCL12/CXCR4 pathway, Molecular and cellular biology 32(16) (2012) 3242-3252.
38. J.E. Vance, G. Tasseva, Formation and function of phosphatidylserine and phosphatidylethanolamine in mammalian cells, Biochimica et Biophysica Acta (BBA)-Molecular and Cell Biology of Lipids 1831(3) (2013) 543-554.
39. J.H.S. Kabarowski, Y. Xu, O.N. Witte, Lysophosphatidylcholine as a ligand for immunoregulation, Biochemical pharmacology 64(2) (2002) 161-167.
40. A.R. Tall, L.J.N.R.I. Yvan-Charvet, Cholesterol, inflammation and innate immunity, 15(2) (2015) 104-116.
41. K. Öztürk, M. Kaplan, S. Çalış, Effects of nanoparticle size, shape, and zeta potential on drug delivery, International journal of pharmaceutics 666 (2024) 124799.
42. F. Motsoene, H. Abrahamse, S.S.D. Kumar, Multifunctional lipid-based nanoparticles for wound healing and antibacterial applications: A review, Advances in colloid and interface science 321 (2023) 103002.